Materials Research Express

PAPER • OPEN ACCESS

Surface modification of AISI-304 steel by ZnO synthesis using cathodic cage plasma deposition

To cite this article: W Nogueira Junior *et al* 2021 *Mater. Res. Express* **8** 096403

IOP Publishing Mater. Res. Express 8 (2021) 096403 https://doi.org/10.1088/2053-1591/ac2443

Materials Research Express

CrossMark

OPEN ACCESS

RECEIVED
17 August 2021

REVISED
28 August 2021

ACCEPTED FOR PUBLICATION
7 September 2021

PUBLISHED
15 September 2021

PAPER

Surface modification of AISI-304 steel by ZnO synthesis using cathodic cage plasma deposition

W Nogueira Junior[1], M Naeem[2], T H C Costa[3], J C Díaz-Guillén[4], M R Díaz-Guillén[5], Javed Iqbal[6,7], Mohsan Jelani[8] and R R M Sousa[1]

[1] Advanced Materials Interdisciplinary Laboratory (LIMAV) - Postgraduate Program in Materials Science and Engineering - Federal University of Piaui (UFPI), Teresina, PI, Brazil
[2] Department of Physics, Women University of Azad Jammu and Kashmir, Bagh, Pakistan
[3] Mechanical Departament—Federal, University of Rio Grande, do Norte (UFRN), Natal, RN, Brazil
[4] CONACYT-Corporación Mexicana de Investigación en Materiales, 25290 Saltillo Coahuila, Mexico
[5] Instituto Nacional de Electricidad y Energías Limpias. Morelos, Mexico
[6] Department of Physics, University of Azad Jammu and Kashmir, Muzaffarabad, Pakistan
[7] University of Latvia, Raina bulvaris 19, Riga LV-1586, Latvia
[8] Department of Physics, University of Kotli, Azad Jammu and Kashmir, Kotli, Pakistan

E-mail: mnaeem@wuajk.edu.pk and naeem.plasma@gmail.com

Keywords: cathodic cage plasma deposition, zinc-oxide, austenitic stainless steel, wear resistance

Abstract

Zinc-oxide (ZnO), a solid lubricant coating, can increase the wear resistance of steels by working as a self-lubricant. In this study, ZnO film is synthesized using the cathodic cage plasma deposition (CCPD) technique, using galvanized steel cathodic cage (steel cage with zinc coating). The effect of gas composition (H_2 is added in Ar-O_2) is investigated to optimize the film properties. The surface hardness is increased more than twice in each processing condition. The deposited film shows ZnO phases for samples treated with low hydrogen contents and a combination of ZnO and magnetite phase (Fe_3O_4) with higher hydrogen contents. The thickness of film reduced from 1.28 μm to 0.5 μm by increasing the hydrogen composition. The wear resistance is expressively increased by film deposition, and the abrasive wear mechanism is changed to an adhesive wear mechanism. A significant decrease in wear rate is observed, specifically by increasing the hydrogen contents. The friction coefficient as a function of sliding distance is smoother and lower than the base material in each condition. This study suggests that the CCPD technique can effectively deposit the solid lubricant coating of ZnO, and it can be used to enhance the tribological properties of steel samples. Moreover, this technique is convenient due to its better deposition efficiency, eco-friendly (no chemicals are involved), simple and relatively low-cost equipment, and low processing temperature. Thus, it can be advantageous for industrial sectors interested in materials with exceptional tribological properties.

1. Introduction

AISI-304 austenitic stainless steels are used in several industrial applications due to their adequate corrosion resistance. Besides corrosion resistance, outstanding mechanical and tribological properties are compulsory to fulfill the industrial requirements [1]. Unfortunately, these materials are unsuitable for motion-contact parts due to their inadequate surface hardness, poor resistance to abrasive and scratching wear behavior [2]. Due to broad applications in industry, the surface modification of stainless steel is under serious consideration for several decades to enhance its hardness and wear resistance [3]. It includes the thermochemical diffusion techniques (in which small size atoms are diffused in the substrate, including nitriding, carburizing, and nitrocarburizing) and hard film deposition [4, 5]. The thermochemical diffusion techniques are more favorable due to better adhesion, and no detachment of layer occurs.

The wear resistance of steels in the motion-contact parts can be enhanced by reducing the friction of moving parts by introducing self-lubricating coatings or solid lubricants [1, 6]. The mechanical and tribological properties of steels can be improved by depositing the hard coatings, which can resist plastic deformation. However, sometimes such coatings cannot improve tribological performance due to substrate stresses [1]. In contrast, solid lubricant coatings are preferable in automobile and aerospace industries to enhance the tribological performance of steels. Zinc-oxide (ZnO), an active member of solid lubricant coatings, can reduce the wear rate and friction coefficient by its lubricating performance [7–9].

The oxidation of metals, including steels by conventional plasma technique, is considered for several decades [10, 11]. It involves the direct bombardment of ions on the surface of samples, removal of material from the sample surface, and its redeposition in the form of metal oxide [11]. However, this technique can deposit only the oxide layer of sample material, and it is not possible to deposit metal oxide layer of some other material than the sample material. Moreover, this system's working depends on direct bombardment on the sample surface, which may cause damage by overheating, and the deposited layer is not homogeneous (due to edge effect) [12]. The limitations associated with conventional plasma systems were addressed two decades ago by introducing a cathodic cage plasma deposition system (CCPD) [13]. Its working is based on sputtering from a cathodic cage (a metal screen that covers the sample surface), and thus it can resolve edge effect issues [12].

Cathodic cage plasma deposition and cathodic cage plasma nitriding (CCPN) working is based on the same principle [14, 15]. However, in this technique, the hollow-cathode effect simultaneously happens across the cathodic cage at a specific processing pressure [14, 15]. The working mechanism of CCPN is proposed in several models. It is mainly based on the sputtering of cage material and its redeposition on the sample surface by reacting with processing gases [16–19]. Recently, Fraczek *et al* [20] suggested the following steps are involved: metal atoms detachment from cage due to ions bombardment into plasma area, reaction with gases atoms and its redeposition on the sample surface. As in this system, the redeposition of cage material is involved. Thus, a layer of the cage material can be deposited on the sample surface. Due to this factor, it is usually referred to as cathodic cage plasma deposition technique [21]. It is widely used to deposit several materials, including aluminum [22], copper [23], silver [24], titanium [25], chromium [26], and nickel [27], to attain various antibacterial, corrosion, and wear resistance properties. Recently Naeem *et al* [28] reported improvement in surface properties of AISI-316 steel sample by depositing molybdenum oxide assisted with CCPD. However, the synthesis of ZnO by using CCPD is not reported so far, to the best of our information.

Pal *et al* [29] synthesized ZnO thin films on stainless steel using the sol-gel route and found that film exhibits good mechanical properties. Essa *et al* [1] used ZnO film as a solid lubricant on steel samples and found that the hardness of steel increased up to 28%. Additionally, the wear rate was reduced by 70% and the friction coefficient by 52% in the presence of this lubricant coating. Basiaga *et al* [30] investigated the mechanical properties of ZnO film deposited by atomic layer deposition on 316LVM steel samples. They suggested improvement in mechanical properties of steel with antibacterial features, and thus it can be used as implants in bone surgery. Staszuk *et al* [31] deposited ZnO coatings on steel samples by atomic layer deposition and reported improved corrosion resistance and wear resistance. Considering these reports, the ZnO films exhibit exceptional mechanical, corrosion, tribological, and antibacterial properties, and thus the synthesis of ZnO films by CCPD is predicted to be of considerable importance.

This study aims to synthesize ZnO film by CCPD and investigate its hardness, structural and wear properties. The films are deposited by changing the composition of hydrogen gas in admixture, and its effect on surface properties is compared.

2. Experimental details

The AISI-304 austenitic stainless steel samples with a cubic geometry of thickness 5 mm and the dimension of 10 mm × 10 mm are used in this study. The composition of used samples was (wt%) 18.9 Cr, 9.20 Ni, 2 Mn, 0.8 Si, 0.05C, 0.02 P, 0.02 S, and Fe (balance). Initially, the samples were cut from a sheet in described dimension; mirror-polished by emery paper with different sizes ranging (400–2500), and finally polished with alumina power and cleaned with running water.

A laboratory-scale cathodic cage plasma deposition reactor with a cylindrical geometry was used in this study, as reported [28]. The probability of edge effect due to ions bombardment on samples surface is reduced by keeping samples on alumina plate (i.e., floating potential) and placed inside the cage. The cage was made up of stainless steel having a zinc coating deposited by galvanizing technique. A new cathodic cage was used to deposit ZnO on each sample to investigate the effect of gasses composition accurately. The cage was cylindrical with a height of 40 mm and a radius 35 mm, having uniformly distributed holes of 4 mm radius. The samples were pre-sputtered to remove the surface contaminations by generating an argon-hydrogen (equal ratio) mixture discharge at 250 °C for 1 h. In ZnO film deposition, the concentration of hydrogen was changed, and detailed conditions are given in table 1.

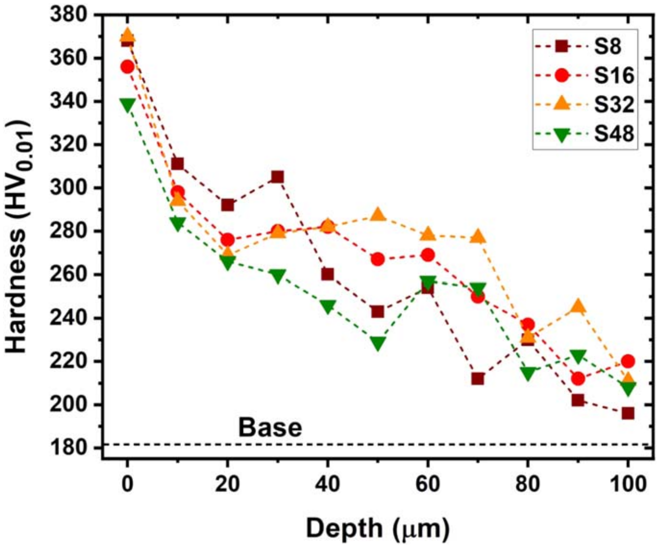

Figure 1. Surface microhardness of base material and zinc-oxide deposited samples under various conditions.

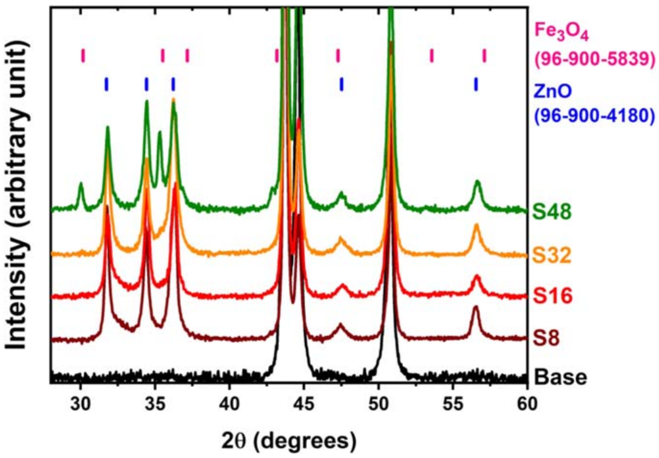

Figure 2. Normal XRD pattern of base material and zinc-oxide deposited samples under various conditions.

Table 1. Labeling of samples used to deposit zinc-oxide on AISI-304 steel samples under various conditions.

Sample Labeling	Hydrogen concentration (sccm) in argon (16 sccm)—oxygen (16 sccm)	Hydrogen (%)	Pressure (Pa)	Temperature (°C)	Time (h)
S8	8	20	110	320	3
S16	16	33	130		
S32	32	50	200		
S48	48	60	400		

Numerous techniques characterized the films: the surface microhardness was evaluated by the Durometer model ISH-TDV 1000 (INSIZE) using a load of 10gf and a dwell time of 15 s. The XRD analysis of ZnO deposited samples was done by Cu-Kα radiation source. The target tube was operated with 40 mA current and 45 kV voltage and scanned in 25°–60°. The detailed phase's structure was analyzed by grazing angle X-ray diffraction (GIXRD) with different incidence angles 0.3°, 1°, 3°, and 5°. The surface of the deposited film and its cross-sectional analysis were done by Tescan model Mira 3 Scanning Electron Microscopy and corresponding elemental composition by energy dispersive spectroscopy (EDS). A dry ball-on-disc wear tester examined the wear performance of deposited films. The wear was analyzed using an alumina ball of 6 mm diameter, track radius 5 mm, speed of 5 cm s^{-1}, at normal load of 1N, and a total sliding distance of 100 m. The wear volume was

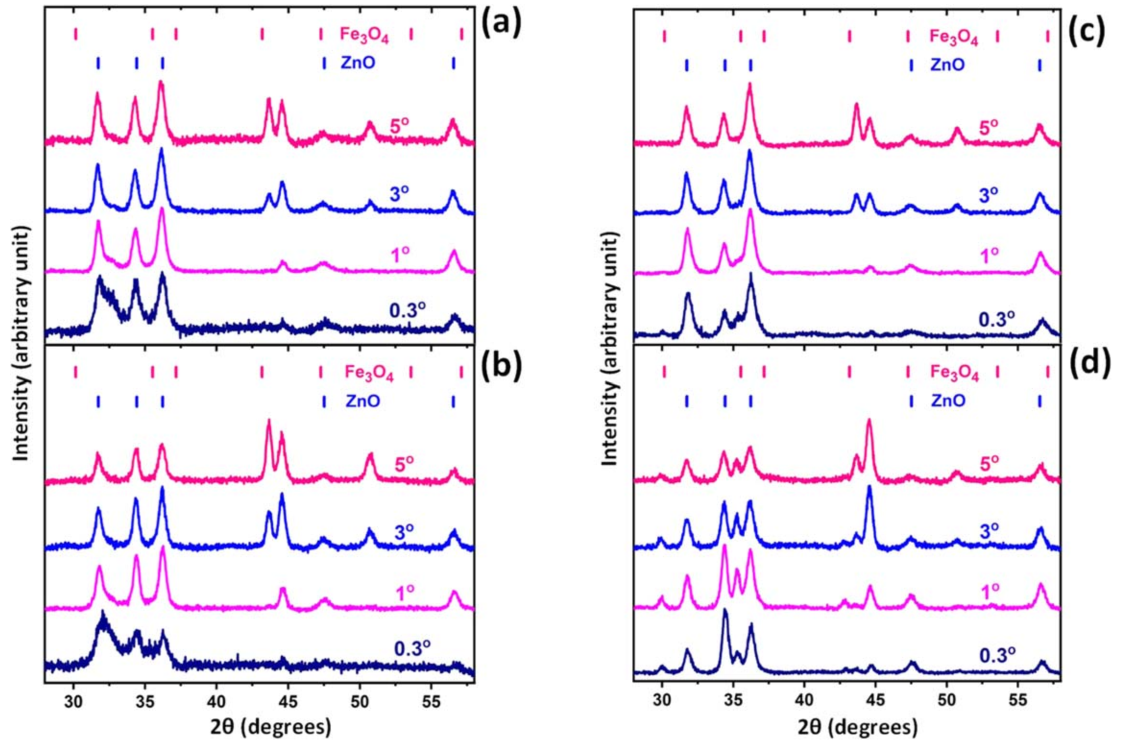

Figure 3. GIXRD pattern of base material and zinc-oxide deposited samples at various grazing angles (a) sample S8, (b) sample S16, (c) sample S32, (d) sample S48.

calculated by standard ASTM G99, and more details regarding wear rates can be found in the previous report [26].

3. Results and discussion

The hardness of ZnO deposited samples corresponding to the depth of the sample is illustrated in figure 1. The hardness profile is also compared with the hardness of the base material (~182 HV). The hardness is found to be increased by ZnO deposition under each deposition condition. The highest surface hardness achieved is up to 370 HV, around two times the hardness of base material. In a previous report, Essa *et al* [1] used the spark plasma sintering (SPS) technique to deposit ZnO film on M50 steel samples, and hardness was increased up to 28% of the base sample. In the CCPD technique, no complicated processes are involved (such as heat treatment, sintering, prepared samples polishing), and also achieved hardness is far higher (105% of base material) than previous report [1].

The structural changes on the surface by film deposition are examined by XRD analysis. The normal XRD pattern of base material and ZnO film deposited samples with various processing conditions is depicted in figure 2. The base material contains an iron phase (austenite phase with a minor amount of martensite phase), expected for the AISI-304 sample [32]. The treated samples with low hydrogen contents (S8, S16, and S32) show the significant presence of the ZnO phase corresponding to crystallographic open data (COD) (96-900-58390. On the other hand, the sample treated with higher hydrogen contents (S48) shows the additional presence of iron oxide (Fe_3O_4, 96-900-5839) with ZnO phases. As here, the cathodic cage of galvanized steel is used, and in each experiment, a new cathodic cage is used, and thus the iron oxide is formed at higher depth due to the presence of iron from the substrate. This assumption can be clarified by using GIXRD analysis, as presented in figure 3. The GIXRD pattern is recorded at various incidence angles (0.3°–5°) to evaluate the changes in phase structure with change in depth. Figures 3(a)–(c) show no significant change in phases is observed with a change in angle, and all samples contain ZnO phases. In contrast, figure 3(d) shows that a small amount of iron oxide is present at 0.3°, and its intensity increases with an increase in grazing angle. It indicates that the top layer in this sample is also composed of the ZnO phase, and while moving to higher depth, iron oxide is also appearing. It is probably caused by the formation of thin ZnO film (which will be justified later by cross-sectional SEM analysis). The formation of ZnO can be ascribed to the sputtering of Zn atoms from the galvanized cathodic cage due to the bombardment of processing gas ions. Then the combination of sputtered Zn with processing gas oxygen atoms

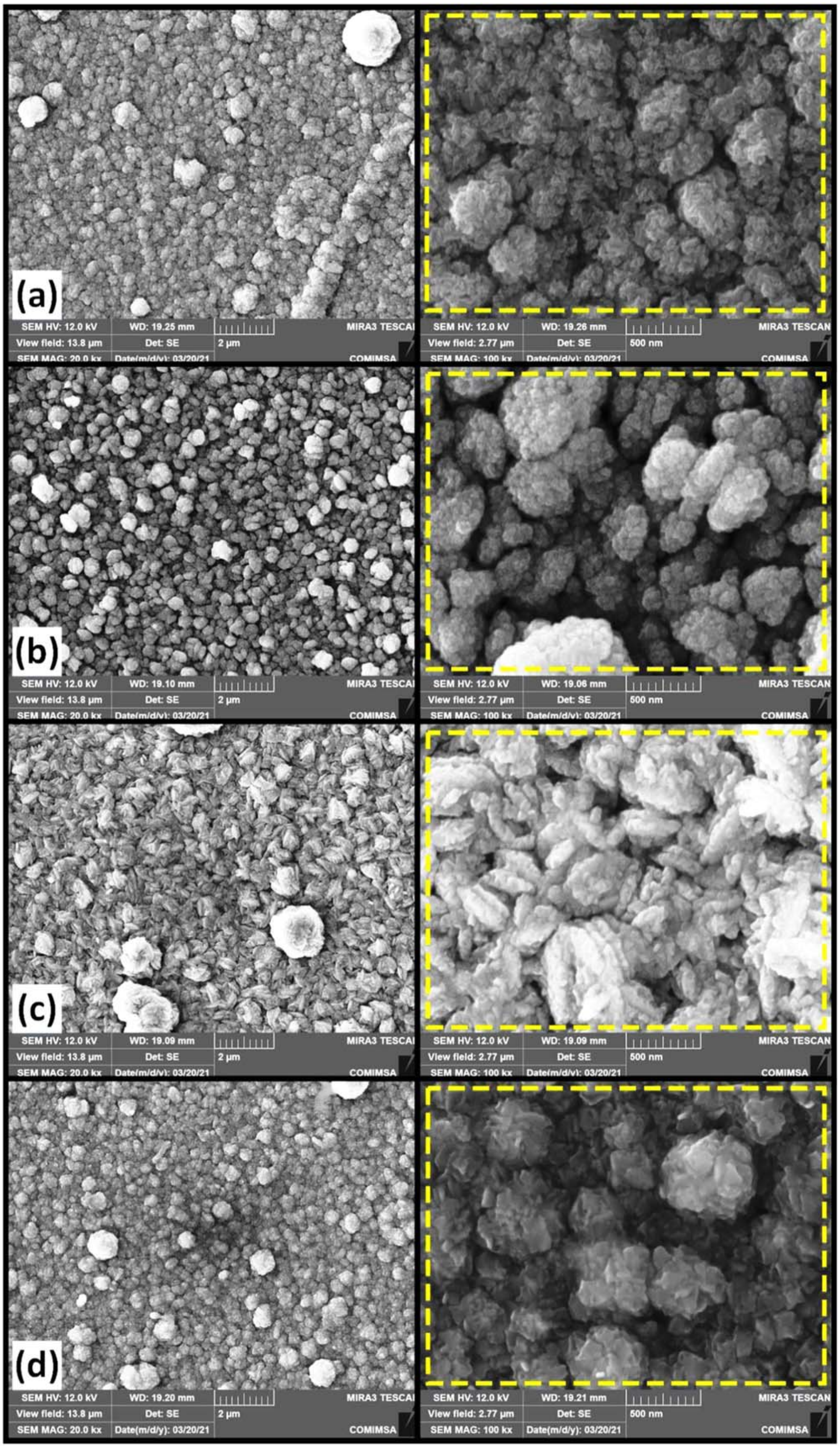

Figure 4. Surface SEM images of zinc-oxide deposited samples under various conditions, (a) sample S8, (a) sample S8, (b) sample S16, (c) sample S32, (d) sample S48.

occurs, and finally, ZnO is deposited on the surface of samples [20]. Here, samples are kept at a floating potential, and thus the probability of iron sputtering from the surface of the sample can be ignored [28].

The surface images of treated samples are presented in figure 4. It depicts that surface is covered with particles with a slight difference in orientation and distribution in each condition. Initially, when the

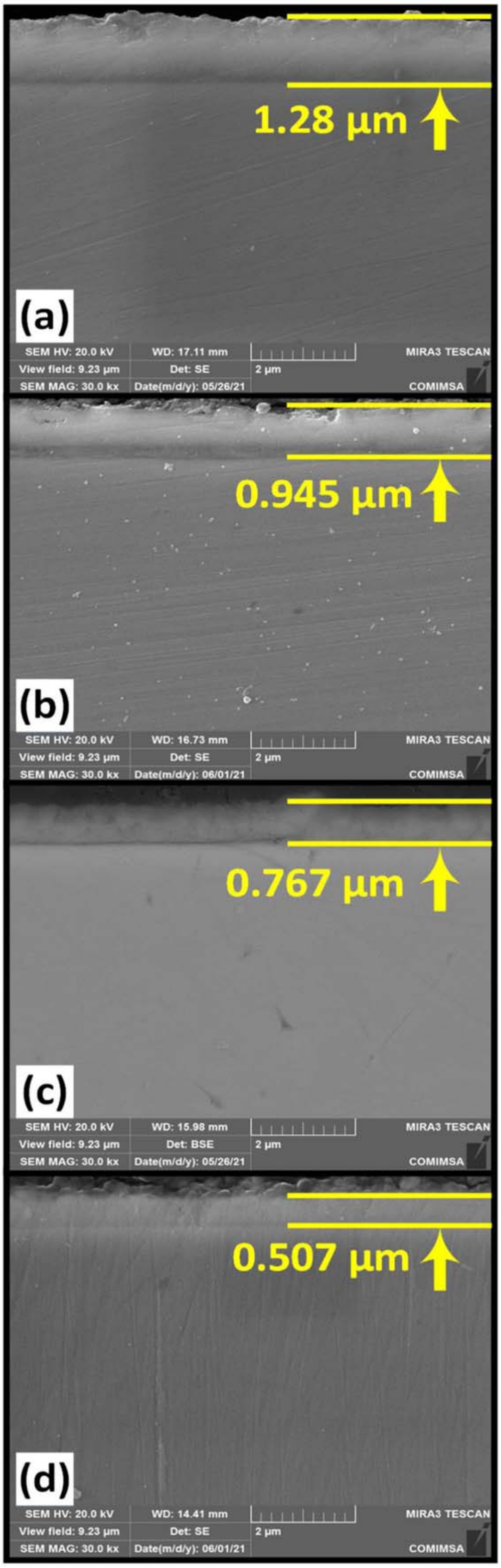

Figure 5. Cross-sectional SEM images of zinc-oxide deposited samples under various conditions, (a) sample S8, (b) sample S16, (c) sample S32, (d) sample S48.

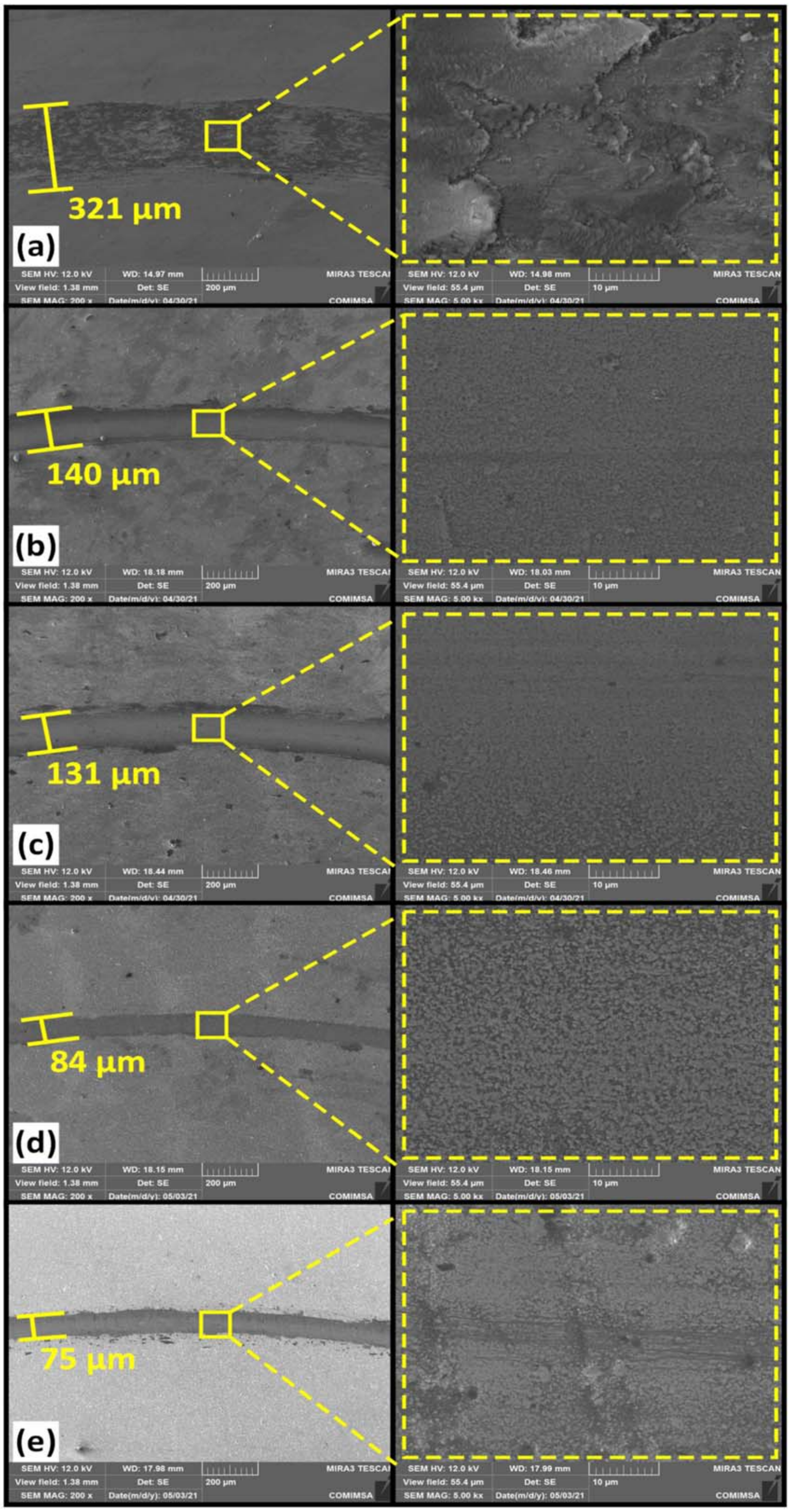

Figure 6. Wear tracks of zinc-oxide deposited samples under various conditions, (a) base material, (b) sample S8, (c) sample S16, (d) sample S32, (e) sample S48.

concentration of hydrogen is small (figures (a)–(c)), the particles are more randomly oriented, and the size distribution is non-uniform. In contrast, the surface is uniformly covered with a homogeneous distribution of particles in the sample treated with higher hydrogen contents (figure 4(d)). This difference in surface appearance can be ascribed to the change in gases composition and the corresponding change in pressure. As in this gases mixture, the sputtering yield due to positive ions bombardment mainly depends on positive argon ions. Thus, a higher sputtering rate is predicted when higher argon ions are present in discharge [33]. When hydrogen content is low (i.e., argon percentage in the mixture is higher), the rate of cage sputtering is higher due to argon ions

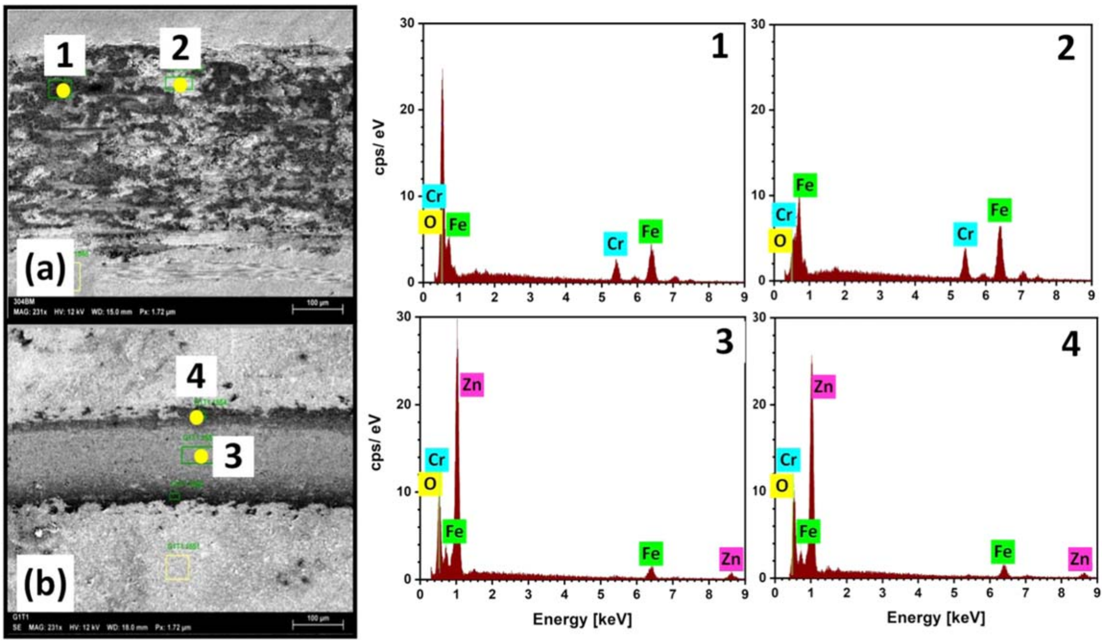

Figure 7. Worn tracks obtained by FESEM of (a) base material (b) S8 sample along with corresponding EDS spectra of different region on tracks.

sputtering. Thus, the film deposition rate is higher [33], and particles are not distributed in an ordered arrangement. When hydrogen is increased, the rate of cage sputtering is reduced, and sputtered material from the cage has enough time to be distributed in a regular arrangement and uniform distribution. Besides the change in gases composition, the corresponding change in pressure is also responsible for the change in surface appearance. With the increase in pressure, the mean free path and mobility of ions decreases; as a result, the number of ions that reach cage holes is reduced, which is accountable for the hollow cathode effect [34]. This statement can be supported later by analyzing the thickness of film using cross-sectional SEM images. The surface images show that particles are closely spaced in each condition, and the deposited film is non-porous. The cross-sectional SEM images of film deposited samples are depicted in figure 5. It shows that the film thickness is 1.28 μm for the S8 sample, and it decreases with the addition of hydrogen contents. The decrease in thickness of the deposited film can be ascribed to the reduction in argon percentage in gases admixture (because argon mainly acts as a sputtering gas) as well as corresponding increase in pressure. Thus argon sputtering yield decreases, as predicted in XRD and SEM observation. Thus, cross-sectional images support the previous assumptions that the rate of cage sputtering decreases when hydrogen percentage is increased in the gas mixture, and thus film thickness decreases. Also, these images show that deposited film is dense and homogeneous in each processing condition. Besides this, when the pressure is increased, the film deposition rate decreases due to a decrease in ions mobility, as reported by Sousa *et al* [34] in a similar pressure range.

The dry sliding wear of base material and treated samples are analyzed using a ball-on-disc wear tester, and dramatic improvement in wear resistance is observed. This improvement in wear resistance can be attributed as ZnO film belongs to the family of solid lubricants, thus reducing wear rate by their lubricating performance [35]. The worn tracks of base material and ZnO deposited samples are depicted in figure 6. The grooves and ridges are induced on the base material parallel to the sliding direction of the ball. This pattern is induced by micro-ploughing of the substrate, plastic deformation, and material detached from the worn surface [36]. The high-resolution image reveals that the detached material is present on the worn track, indicating abrasive wear behavior. Also, the worn track shows the smearing of material and dark patches are visible. This is clarified by EDS analysis of bright and dark patches as presented in figure 7, clarifying that dark patches are oxidized. The oxidation on the worn track of the untreated sample is caused by local high-temperature oxidation reaction due to a compact contact among sliding ball and sample. On the other hand, the treated samples show that tracks are significantly narrower; this indicates improved wear performance. Very small smearing is detected (at the boundaries of the track), finer grooves and no craters are observed due to improved wear resistance by the solid-lubricant film. By changing the deposition condition, a slight improvement in wear resistance is observed, which

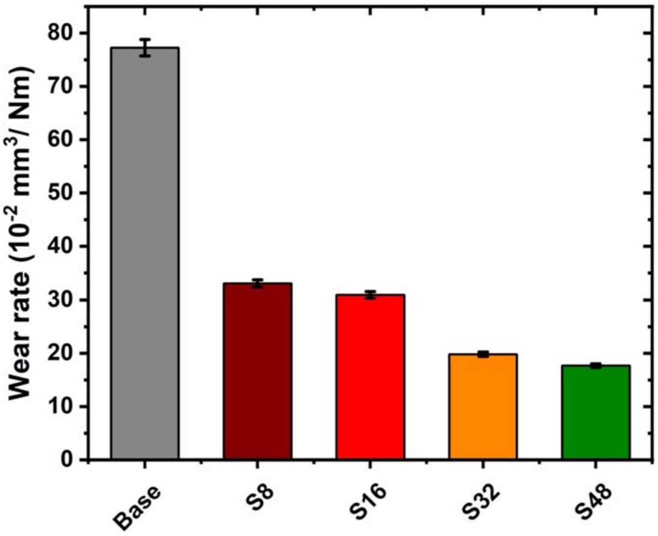

Figure 8. Wear rates of zinc-oxide deposited samples under various conditions.

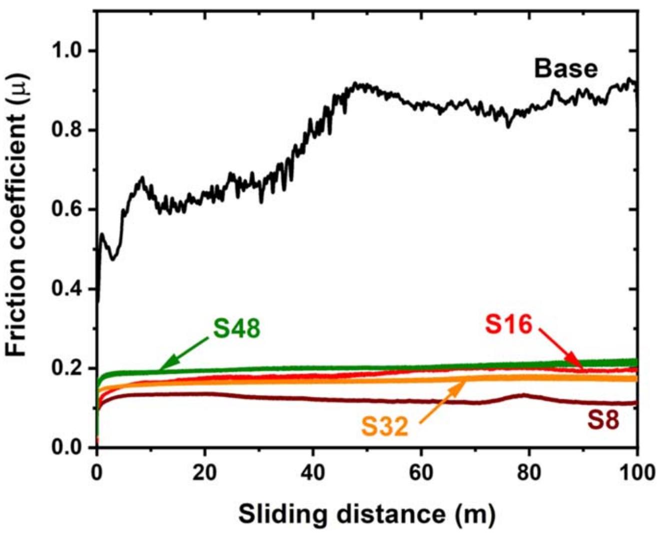

Figure 9. Variation of friction coefficient versus sliding distance of zinc-oxide deposited samples under various conditions.

may be caused by the formation of a more dense film, as observed in SEM analysis in figure 4. The smeared region at the track's edges and central region is distinguished by SEM analysis as presented in figure 7(b), which shows no significant change in both regions. It indicates that the track still contains the dominant amount of Zn and oxygen, and ZnO film is not removed during sliding contact. The quantified wear rates are presented in figure 8, showing a significant decrease in wear rate by ZnO deposition, specifically by using higher hydrogen contents (a minor improvement). The variation of friction coefficient curves as a function of sliding distance is plotted in figure 9, and their averages of the sliding distance of 100 m are plotted in figure 10. The friction coefficient of the untreated sample is fluctuating and is higher than the ZnO deposited samples. The higher values can be ascribed to the low hardness of the sample, and fluctuations can be due to oxidation and removal of the oxide layer, as presented in figure 8 [37]. The friction coefficient of ZnO deposited samples is smooth and lower values. This is further supported by SEM analysis that the surface of these samples is clean, smooth, and non-detectable imperfection. The reduction and smoothness of friction coefficient can be attributed to the lubricating performance of ZnO, which acts as a lubricant during the sliding of the ball and hence improves wear resistance. Thus, this study shows that the wear resistance of AISI-304 steel can be enhanced significantly by ZnO film assisted with the CCPD technique. The obtained increase in hardness is better than previous reports, and this technique is more favorable than the conventional techniques [1, 29].

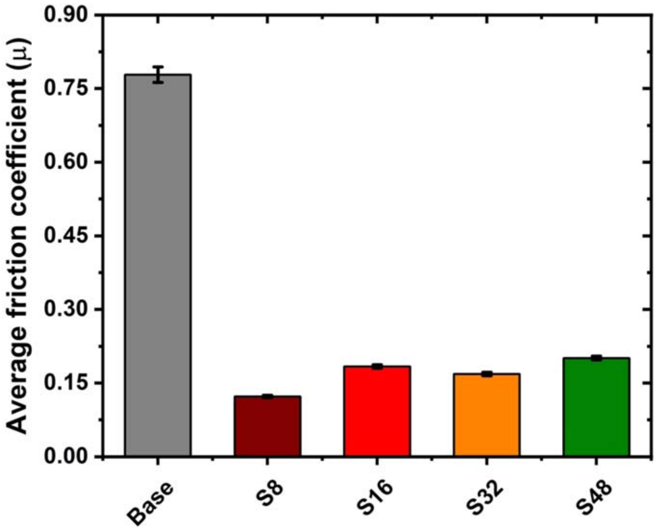

Figure 10. Average friction coefficient of zinc-oxide deposited samples under various conditions.

4. Conclusions and final remarks

The solid-lubricant zinc-oxide film is synthesized on steel samples by cathodic cage plasma deposition (CCPD) to improve the tribological features. The outcomes can be summarized as follow:

1. A solid self-lubricating coating of ZnO is successfully deposited on steel samples by CCPD, and exceptional film characteristics are obtained.
2. The hardness is upgraded more than twice of base material hardness in each condition, with the additional feature of self-lubrication.
3. The deposited film shows the dominant presence of the ZnO phase when deposited by low hydrogen concentration and ZnO-Fe_3O_4 when deposited with higher hydrogen. The iron-containing phases are found to be appeared at higher depth due to the substrate iron contents.
4. The film thickness is reduced while adding a higher amount of hydrogen and the films are almost homogeneous in each condition. The decrease in film thickness by changing processing gases is due to a decrease in argon ions which are mainly responsible for sputtering and the increase in filling pressure.
5. The wear rate is dramatically reduced by film deposition due to its lubricating performance, and the friction coefficient is lower and smoother for the deposited film. The wear mechanism is transferred from abrasive wear to adhesive wear mechanism in the presence of the film.

Besides improving tribological performance and increasing hardness, this system (with larger dimensions) is suitable for industrial applications. Additionally, no chemicals are used, processing time and temperature are relatively small, and the film is homogeneous. Thus, we predict that this study will helpful for industrial applications to improve the tribological performance of steel.

Acknowledgments

RRMS is thankful to National Council for Scientific and Technological Development (CNPq) for partial financial support. JCDG would like to thank the Mexican National Council for Science and Technology (CONACYT) for the financial support to carry out this research work (Grant No. CB-2015 257705). Dr Javed Iqbal is thankful to European Regional Development Fund (Project No.1.1.1.5/19/A/003) for the development of quantum optics and photonics at the university of Latvia.

Data availability statement

All data that support the findings of this study are included within the article (and any supplementary files).

Conflict of interest statement

The authors declare no conflict of interest.

ORCID iDs

M Naeem https://orcid.org/0000-0001-9657-513X
M R Díaz-Guillén https://orcid.org/0000-0003-0174-993X
Mohsan Jelani https://orcid.org/0000-0002-7106-113X
R R M Sousa https://orcid.org/0000-0003-2062-6505

References

[1] Essa F A, Zhang Q, Huang X, Ibrahim A M M, Ali M K A, Abdelkareem M A A and Elagouz A 2017 Improved friction and wear of M50 steel composites incorporated with ZnO as a solid lubricant with different concentrations under different loads *J. Mater. Eng. Perform.* **26** 4855–66

[2] Naeem M, Raza H A, Shafiq M, Zaka-ul-Islam M, Iqbal J, Díaz-Guilléne J C and Zakaullah M 2017 Effect of pulsed duty cycle control on tribological and corrosion properties of AISI-316 in cathodic cage plasma nitriding *Mater. Res. Express* **4** 116507

[3] Angsuseranee N, Watcharasresomroeng B, Bunyawanichkul P and Chartniyom S 2020 Tribological behavior of tool steel substrate and solid films against 304 BA austenitic stainless steel under dry sliding *Advances in Tribology* **2020** 8845548

[4] Araujo A G F, Naeem M, Araujo L N M, Costa T H C, Khan K H, Díaz-Guillén J C, Iqbal J, Liborio M S and Sousa R R M 2020 Design, manufacturing and plasma nitriding of AISI-M2 steel forming tool and its performance analysis *Journal of Materials Research and Technology* **9** 14517–27

[5] Naeem M, Díaz-Guillén J C, Akram M, Iqbal J, Naz M Y and Shafiq M 2020 Novel active screen plasma nitriding of aluminum using aluminum cathodic CAGE *Surf. Rev. Lett.* **27** 1950118

[6] Koutsomichalis A, Vaxevanidis N, Petropoulos G, Xatzaki E, Mourlas A and Antoniou S 2009 Tribological coatings for aerospace applications and the case of WC–Co plasma spray coatings *Tribology in Industry* **31** 37–42

[7] Dikici T 2017 Temperature-dependent growth of ZnO structures by thermal oxidation of Zn coatings electrodeposited on steel substrates and their photocatalytic activities *Ceram. Int.* **43** 8289–93

[8] Wang X, Lu H, Liu W, Guo M and Zhang M 2017 Electrodeposition of flexible stainless steel mesh supported ZnO nanorod arrays with enhanced photocatalytic performance *Ceram. Int.* **43** 6460–6

[9] Da B, Yaxuan L, Vasu A T, Yongxin G, Hao T, Yongwu Z and Yongguang W 2021 Improving tribocorrosion performance of chemically bonded ceramic phosphate coating reinforced by GO-ZnO *Ceram. Int.* **47** 15722–31

[10] Chang R P H 1983 Plasma oxidation of semiconductor and metal surfaces *Passivity of Metals and Semiconductorsed.* ed M Froment (Amsterdam: Elsevier) pp 437–44

[11] Díaz-Guillén J C, Zamarripa-Piña J S, Granda-Gutiérrez E E, González-Albarrán M A, Díaz-Guillén J A, Pérez-Aguilar S I and Candelas-Ramírez J 2013 Increase of salt fog corrosion resistance of plasma nitrided steel by pulsed plasma post-oxidation *Int. J. Modern. Eng. Res.* **3** 386–90

[12] Olzon-Dionysio M, Campos M, Kapp M, de Souza S and de Souza S D 2010 Influences of plasma nitriding edge effect on properties of 316 L stainless steel *Surf. Coat. Technol.* **204** 3623–8

[13] Li C, Bell T and Dong H 2002 A study of active screen plasma nitriding *Surf. Eng.* **18** 174–81

[14] Alves C, de Araújo F O and de Sousa R R M 2016 Gas and plasma nitriding versus nitrocarburizing processes *Encyclopedia of Iron, Steel, and Their Alloysed.* (Boca Raton, FL: CRC Press) pp 1316–27

[15] Alves C Jr, De Araújo F O, Ribeiro K J B, Da Costa J A P, Sousa R R M D and De Sousa R S 2006 Use of cathodic cage in plasma nitriding *Surf. Coat. Technol.* **201** 2450–4

[16] Saeed A, Khan A, Jan F, Abrar M, Khalid M and Zakaullah M 2013 Validity of 'sputtering and re-condensation' model in active screen cage plasma nitriding process *Appl. Surf. Sci.* **273** 173–8

[17] Gallo S C and Dong H 2009 On the fundamental mechanisms of active screen plasma nitriding *Vacuum* **84** 321–5

[18] Hubbard P, McCulloch D G, Doyle E D, Dowey S J and Georges J N 2006 A fundamental contribution to a study of the active screen plasma nitriding process *BHM Berg- und Hüttenmännische Monatshefte* **151** 441–5

[19] Hubbard P, Partridge J, Doyle E, McCulloch D, Taylor M and Dowey S 2010 Investigation of nitrogen mass transfer within an industrial plasma nitriding system I: the role of surface deposits *Surf. Coat. Technol.* **204** 1145–50

[20] Fraczek T, Ogorek M, Skuza Z and Prusak R 2020 Mechanism of ion nitriding of 316L austenitic steel by active screen method in a hydrogen-nitrogen atmosphere *Int. J. Adv. Manuf. Technol.* **109** 1357–68

[21] de Sousa R R M, Sato P S, Viana B C, Alves C Jr, Nishimoto A and Nascente P A P 2015 Cathodic cage plasma deposition of TiN and TiO_2 thin films on silicon substrates *Journal of Vacuum Science & Technology A* **33** 041502

[22] Naeem M, Shafiq M, Zaka-ul-Islam M, Bashir M I, Díaz-Guillén J C, Lopez-Badillo C M and Zakaullah M 2017 Novel duplex cathodic cage plasma nitriding of non-alloyed steel using aluminum and austenite steel cathodic cages *J. Alloys Compd.* **721** 307–11

[23] Zaka-ul-Islam M, Naeem M, Shafiq M, Sitara, Al-Rajab A J and Zakaullah M 2017 Active screen cage pulsed dc discharge for implanting copper in polytetrafluoroethylene (PTFE) *Mater. Res. Express* **4** 075304

[24] Lin K, Li X, Tian L and Dong H 2015 Active screen plasma surface co-alloying treatments of 316 stainless steel with nitrogen and silver for fuel cell bipolar plates *Surf. Coat. Technol.* **283** 122–8

[25] Silva S S D, Bottoni C D L R, Gontijo L C and Ferreira S O 2017 Plasma deposition of titanium nitride thin films under the effect of hollow cathode length in cathodic cage *Matéria (Rio de Janeiro)* **22** 11857

[26] Naeem M, Shafiq M, Zaka-ul-Islam M, Ashiq A, Díaz-Guillén J C, Shahzad M and Zakaullah M 2016 Enhanced surface properties of plain carbon steel using plasma nitriding with austenitic steel cathodic cage *Mater. Des.* **108** 745–53

[27] Morell-Pacheco A, Kim H, Wang T, Shiau C-H, Balerio R, Gabriel A and Shao L 2020 Ni coating on 316L stainless steel using cage plasma treatment: Feasibility and swelling studies *J. Nucl. Mater.* **540** 152385

[28] Naeem M, Fortaleza V C, Serra P L C, Lima C L, Costa T H C, Sousa R R M, Díaz-Guillén J C, Mancillas-Salas S and Iqbal J 2021 Synthesis of molybdenum oxide on AISI-316 steel using cathodic cage plasma deposition at cathodic and floating potential *Surf. Coat. Technol.* **406** 126650

[29] Pal N, Aggrawal A, Jayaganthan R and Chowdhury R 2015 Effect of coating thickness on the mechanical behavior of ZnO thin films on stainless steel prepared by Sol-gel route *6th International Conf. On 'Recent Trends in Applied Physical, Chemical Sciences, Mathematical/ Statistical and Environmental Dynamics'* (PCME)

[30] Basiaga M, Walke W, Sambok-Kiełbowicz A, Paszenda Z, Kaczmarek M, Taratuta A, Szindler M and Ziębowicz B 2020 The influence of the parameters of the zinc oxide layer deposition process using the atomic layer deposition method on the physical and mechanical properties of 316LVM steel *Materialwiss. Werkstofftech.* **51** 624–30

[31] Staszuk M, Pakuła D, Reimann Ł, Król M, Basiaga M, Mysłek D and Kříž A 2020 Structure and properties of ZnO coatings obtained by atomic layer deposition (ALD) method on a Cr–Ni–Mo steel substrate type *Materials* **13** 4223

[32] Naeem M, Iqbal J, Zakaullah M, Shafiq M, Mujahid Z I, Díaz-Guillén J C, Lopez-Badillo C M, Sousa R R M and Khan M A 2019 Enhanced wear and corrosion resistance of AISI-304 steel by duplex cathodic cage plasma treatment *Surf. Coat. Technol.* **375** 34–45

[33] Naeem M, Iqbal J, Abrar M, Khan K H, Díaz-Guillén J C, Lopez-Badillo C M, Shafiq M, Zaka-ul-Islam M and Zakaullah M 2018 The effect of argon admixing on nitriding of plain carbon steel in N2 and N2–H2 plasma *Surf. Coat. Technol.* **350** 48–56

[34] de Sousa R R M, de Araújo F O, Gontijo L C, da Costa J A P, Nascimento I O and Alves C Jr 2014 Cathodic cage plasma nitriding of austenitic stainless steel (AISI 316): influence of the working pressure on the nitrided layers properties *Mater. Res.* **17** 427–33

[35] Zhu S, Bi Q, Niu M, Yang J and Liu W 2012 Tribological behavior of NiAl matrix composites with addition of oxides at high temperatures *Wear* **274** 423–34

[36] Zahmatkesh B, Enayati M H and Karimzadeh F 2010 Tribological and microstructural evaluation of friction stir processed Al2024 alloy *Mater. Des.* **31** 4891–6

[37] Dogan H, Findik F and Oztarhan A 2003 Comparative study of wear mechanism of surface treated AISI 316L stainless steel *Industrial Lubrication and Tribology* **55** 76–83